Revelation of the Role of Impurities and Conduction Electron Density in the High Resolution Photoemission Study of Ferromagnetic Hexaborides

Kalobaran Maiti,* V. R. R. Medicherla, Swapnil Patil, and Ravi Shankar Singh

Department of Condensed Matter Physics and Materials Science, Tata Institute of Fundamental Research, Homi Bhabha Road, Colaba, Mumbai 400005, India

(Received 9 May 2007; published 26 December 2007)

We investigate the temperature evolution of the electronic structure of ferromagnetic CaB_6 using ultrahigh resolution photoemission spectroscopy; the electronic structure of paramagnetic LaB_6 is used as a reference. High resolution spectra of CaB_6 reveal a finite density of states at the Fermi level ϵ_F at all the temperatures and evidence of impurity induced localized features in the vicinity of ϵ_F, which are absent in the spectra of LaB_6. Analysis of the high resolution spectra suggests that disorder in the B sublattice inducing partial localization in the mobile electrons and low electron density at ϵ_F is important to achieve ferromagnetism in these systems.

DOI: 10.1103/PhysRevLett.99.266401 PACS numbers: 71.27.+a, 71.23.−k, 71.55.Ak, 75.10.Lp

The discovery of unusual ferromagnetism in hexaborides, MB_6 (M = Ca, Sr, Ba, etc.) [1,2] and in La-doped CaB_6 [3] with a high Curie temperature ($T_C \geq 600$ K) has attracted a great deal of interest due to many interesting fundamental issues associated with this novel phenomena and huge potential in technological applications as well. Strikingly, none of the constituent elements in these compounds possess partially filled d or f levels to manifest ferromagnetism. In addition, the ground state of all the ferromagnetic compositions is very close to the band insulating phase [1–4]. One school believes that ferromagnetism in these systems arises due to the polarization of low density conduction electrons (electron density slightly higher than the limit of Wigner crystallization) [3,5]. Another school describes hexaborides as hole doped excitonic insulators (excitonic model) [6]. The later description was prompted by the observation of a band overlap at X point of the Brillouin zone in *ab initio* calculations [4] and subsequent description of the de Haas–van Alphen and Shubnikov–de Haas results [7–9] within the same framework. However, more recent *ab initio* calculations [10] and x-ray absorption and emission measurements [11] exhibit an insulating phase in CaB_6. Angle resolved photoemission spectroscopic (ARPES) studies indicate an energy gap >1 eV at the X point, which is too high for the suitability of the excitonic model [11,12].

In parallel, investigations by Matsubayashi *et al.* suggest that the ferromagnetism in $Ca_{1-x}La_xB_6$ appears due to Fe impurities coming from the crucibles used for sample preparation [13]. However, the dependence of ferromagnetism on La concentration is curious. Subsequently, several experimental and theoretical studies are carried out to understand the origin of ferromagnetism in these systems. For example, CaB_6 grown using a Ca rich mixture of elements does not exhibit ferromagnetism but becomes weakly paramagnetic along with an increase in low temperature resistivity by more than two orders [1]. This observation suggests that ferromagnetism of the nominally pure system is related to the presence of vacancies in the metal sublattice. CaB_6 grown at different temperatures using high purity CaO and B show large differences in magnetic and resistivity behaviors [14]. A recent study [15] shows that tuning of Ca concentration and/or La doping does not lead to ferromagnetism if the samples are prepared using high purity (99.9999%) boron. Instead, the samples prepared using 99.9% pure boron exhibits ferromagnetism at certain compositions. A theoretical study [16] based on *ab initio* calculations suggests that ferromagnetism in $Ca_{1-x}La_xB_6$ arises due to B_6 vacancy and that the dominant contribution comes from the surface rather than the bulk. Another study attributed ferromagnetism of CaB_6 to sp electrons in narrow impurity bands [17]. A ferromagnetic moment in CaB_6 is observed to depend strongly on defect concentration [18].

It is clear that ferromagnetism in hexaborides is far from understood. In this Letter, we report our results on the evolution of the electronic structure of CaB_6 and LaB_6 in the vicinity of the Fermi level ϵ_F as a function of temperature using state-of-the-art high resolution photoemission spectroscopy. LaB_6 is paramagnetic and, hence, is used as a reference. High resolution spectra of CaB_6 exhibit finite spectral intensity at ϵ_F, despite the fact that it is predicted to be a band insulator. Temperature evolution reveals impurity features below ϵ_F in CaB_6, while LaB_6 exhibits Fermi liquid behavior and a disorder induced dip at ϵ_F.

CaB_6 and LaB_6 were prepared in an arc furnace using 99.7% pure B powder, where all the ingredients were kept in a water cooled high purity OFHC copper hearth (to avoid contaminations due to crucibles) and melted in an ultrahigh pure argon atmosphere. The high quality of the samples was ensured by sharp and intense x-ray diffraction patterns, and EDX-SEM measurements. No trace of foreign elements was found in these samples. The measurements using a high sensitivity vibrating sample magne-

tometer and a SQUID magnetometer exhibit paramagnetic temperature dependence of magnetization of LaB_6 down to 1.8 K. The magnetization vs applied magnetic field curves are shown in Fig. 1. No hysteresis loop is observed for LaB_6. The measurements on CaB_6 exhibit a clear hysteresis loop typical of a ferromagnetic material even at room temperature, suggesting a high Curie temperature of this material. The magnetization curves of all the ingredients (the curve for B powder is shown here) show negligible magnetic moment. This suggests that ferromagnetism in CaB_6 is intrinsic and does not appear due to magnetic impurities. The resistivity of CaB_6 shows metallic temperature dependence (varying between 11 $m\Omega$ cm at 1.8 K to 16 $m\Omega$ cm at 300 K). Photoemission measurements were performed on samples fractured at 4×10^{-11} torr vacuum, using a monochromatized UV source and electron analyzer, SES2002 from Gammadata Scienta, at an energy resolution of 1.4 meV [19]. The temperature variation down to 10 K was achieved by an open cycle He cryostat from Advanced Research Systems, USA. Band structure calculations were carried out using a full potential linearized augmented plane wave method within the local density approximations (LDA) using WIEN2K software [20]. The convergence ($\Delta E < 0.25$ meV/f.u. and $\Delta Q < 10^{-3}$ electronic charge) was achieved considering 1000 k points within the first Brillouin zone.

In Fig. 2(a), we show the valence band spectrum of CaB_6 collected at 10 K using He I radiations. There are two distinct features around 1.5 eV and 3 eV binding energies as also observed in previous ARPES study [12]. Intensity at ϵ_F appears to be zero, suggesting an insulating character of this material with a large gap. We show the calculated total density of states (TDOS) in Fig. 2(b) and various partial density of states (PDOS) in Figs. 2(c) and 2(d). Interestingly, the LDA results exhibit an insulating ground state with an energy gap of about 0.2 eV characterizing CaB_6 as a *band insulator;* the reproduction of the exact band gap may need other considerations [10,21]. It is evident that the TDOS is primarily contributed by B 2p PDOS shown in Fig. 2(c). All other contributions (B 2s, Ca 3d, etc.) are significantly small in this energy range. Similar energy distribution of Ca 3d PDOS and B 2p PDOS, and the features above ϵ_F (not shown here) indicate significant Ca 3d-B 2p covalency. The relative intensity of the features in the calculated results are slightly different from the experimental results presumably due to the fact that the experimental spectra are influenced significantly by the matrix element effects, lifetime broadening of the holes and electrons in addition to various other final states effects, which are not considered in the *ab initio* calculations. Interestingly, the energy positions of the features resemble remarkably well the experimental features. All these results as well as the observation of similar band dispersions in previous studies [12] indicate that the influence from correlation effects is weak as expected for B 2p electrons.

While the spectrum in Fig. 2(a) indicates no intensity at ϵ_F, very high resolution spectra, however, reveal a different scenario. ϵ_F at various temperatures was determined experimentally by the Fermi cutoff measured in Ag mounted on the same sample holder. This is demonstrated in Fig. 3(a), where the valence band spectra of Ag at 300 K and 20 K crosses at ϵ_F. Interestingly, all the spectra of CaB_6 shown in Fig. 3(c) exhibit finite intensity at ϵ_F, which is consistent with the observation of the Fermi surface in de Haas–van Alphen measurements [9]. The 150 K spectrum of CaB_6 exhibits a negative slope near ϵ_F indicating that ϵ_F is pinned above the valence band. The intensity at ϵ_F is very small and presumably arising due to

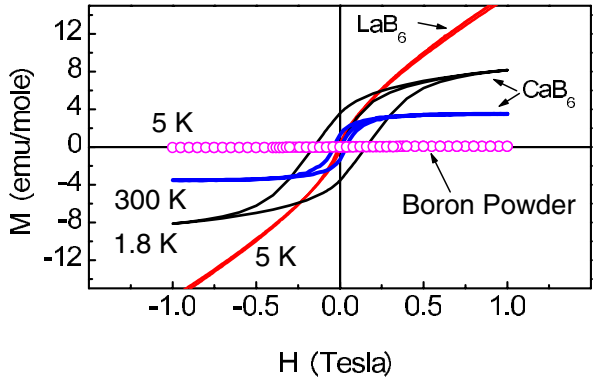

FIG. 1 (color online). Magnetic hysteresis curves of CaB_6, LaB_6, and B powder (purity = 99.7%) used for sample preparation.

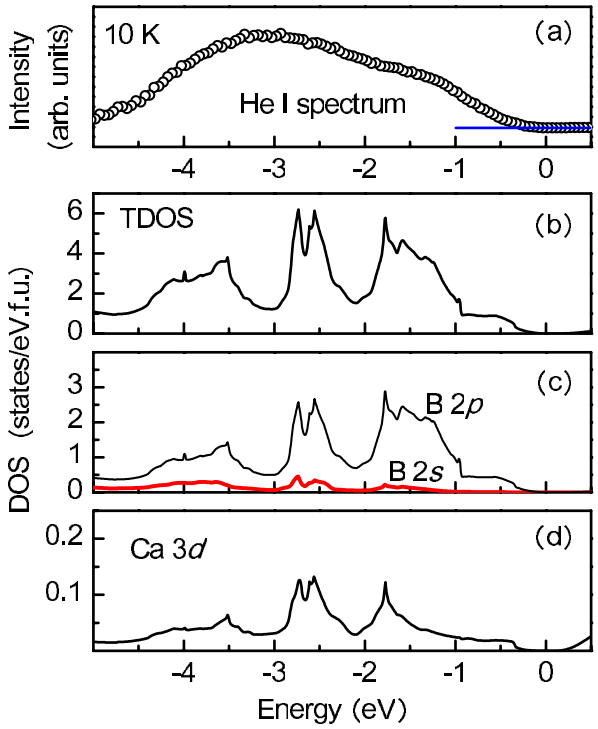

FIG. 2 (color online). (a) Valence band spectrum of CaB_6 at 10 K. Calculated (b) TDOS, (c) B 2s and B 2p PDOS, and (d) Ca 3d PDOS.

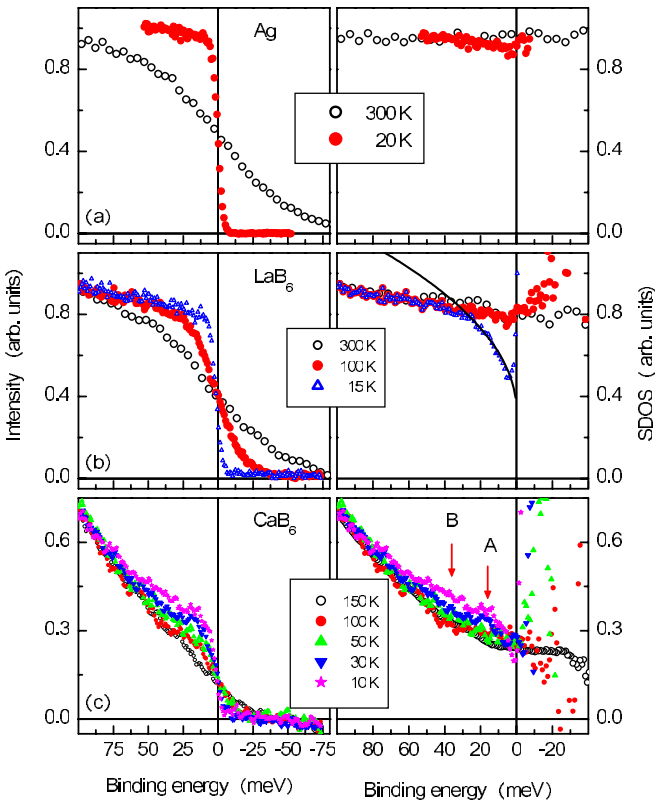

FIG. 3 (color online). He I spectra of (a) Ag, (b) LaB_6, and (c) CaB_6 in the vicinity of ϵ_F. The right panels exhibit SDOS obtained by dividing the spectra in the left panel by the Fermi-Dirac distribution function.

the impurities and/or defects leading to charge carrier doping in this band insulating material.

All the spectra cross each other at ϵ_F as expected from the temperature dependent Fermi-Dirac distribution function. However, the intensity below ϵ_F increases unusually with the decrease in temperature. Such highly anomalous spectral evolution is not observed in LaB_6 as shown in the middle panel of the figure. We have divided all the spectra in the left panel of Fig. 3 by the Fermi-Dirac distribution function. The high energy resolution employed in these measurements introduce negligible resolution broadening in the experimental spectra. Thus, such divided spectral functions are a good representation of the spectral density of states (SDOS) as often observed in other systems [22,23]. SDOS at different temperatures for all the three samples, Ag, LaB_6, and CaB_6, are shown in the right panel of the figure. SDOS of Ag exhibits a flat distribution of intensity as a function of binding energy as expected for bulk Ag. LaB_6 also exhibits essentially flat and temperature independent SDOS down to 100 K. A further decrease in temperature leads to a sharp dip at ϵ_F with a line shape, $I(\epsilon) = I_0 + a|\epsilon - \epsilon_F|^\alpha$, where $\alpha = 0.5$ (solid line in the figure). This suggests that disorder plays an important role in determining the electronic structure in this system [24] in addition to the electron-phonon coupling effect predicted before [25,26].

Strikingly different behavior is observed in CaB_6. The intensity at ϵ_F remains almost unchanged down to the lowest temperature studied. Most interestingly, the intensity below ϵ_F increases gradually with the decrease in temperature. The growing features are manifested by a double peak structure marked by "*A*" and "*B*" in the figure. In order to probe the features more clearly, we have derived the spectral functions at lower temperatures by convoluting the SDOS at 150 K with Fermi-Dirac distribution function. The simulated spectra represented by solid lines are compared with the experimental spectra (symbols) in Fig. 4(a). Clearly, the experimental spectra exhibit much enhanced intensity compared to that expected merely due to the thermal effects included in the Fermi-Dirac distribution function. We have subtracted the 150 K spectrum from all the spectra at low temperatures to find the spectral weight transfer, which are shown in Fig. 4(b). The smooth lines through the points are drawn to guide the eye. The zero intensity at ϵ_F indicates that the DOS at ϵ_F remain essentially unchanged. Two distinctly separable features are observed at about 15 meV and 36 meV binding energies. In Fig. 4(c), we show the difference spectra at

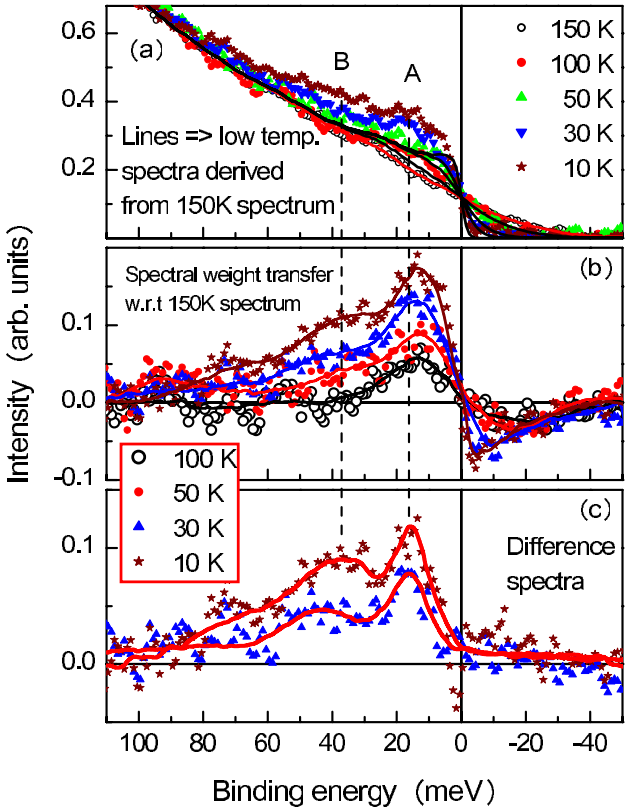

FIG. 4 (color online). (a) He I spectra of CaB_6 at different temperatures. The lines represent the low temperature spectra derived from SDOS at 150 K. (b) The temperature induced spectral weight transfer calculated by subtracting 150 K spectrum from all the other spectra. (c) Difference spectra at 30 K and 10 K obtained by subtracting the lines in (a) from the corresponding raw data.

30 K and 10 K after subtracting corresponding estimated spectral functions shown in Fig. 4(a). Interestingly, the temperature induced changes at the Fermi edge are not visible in Fig. 4(c). This reveals the fact that the delocalized density of states follow the Fermi-Dirac distribution function and may be described within a Fermi liquid picture. The features A and B are weakly localized and manifested at low temperatures due to a lesser degree of thermal excitations.

These results thus clearly suggest that small impurities ($\sim$0.3%) in a B sublattice introduce localized electronic states just above the valence band. The double peak structure and their intensity ratio suggest $2p$ character of the electrons with a spin-orbit splitting of about 20 meV. This is not unlikely, since the valence band is constituted essentially by B $2p$ electronic states. These features are not observed in LaB_6, despite the fact that both the samples are prepared using identical procedures. Instead, the spectra in LaB_6 exhibit a dip at ϵ_F. LaB_6 is a good metal with large conduction electron density ($\approx$1022 cm^{-3}) at ϵ_F, which presumably smears out the local features suggesting that the conduction electron density plays an important role here.

The crystal structure of the hexaborides consists of two interpenetrating cubic lattices formed by metals and B_6 octahedra. The B sublattice is very stable and robust, and essentially B $2p$ electrons determine the electronic properties. The impurities in B introduce significant disorder as clearly observed in LaB_6 in addition to the doping of charge carriers. This has twofold effects. While disorder leads to local moments via the localization effect, the delocalized character of the doped carriers helps to mediate exchange interactions resulting in long range order. This scenario explains the studies performed so far on various samples. For example, it is observed [15] that samples prepared with 99.9999% purity B do not exhibit ferromagnetism despite the tuning of charge carrier density by changing the Ca concentration. It is thus clear that merely change in carrier concentration does not lead to ferromagnetism. On the other hand, samples such as CaB_6, $Ca_{1-\delta}La_xB_6$, and $Ca_{1-x}La_xB_6$ prepared with poorer B purity exhibit ferromagnetism when the carrier concentration is low. In every case, the impurities in the B sublattice, vacancies, and/or La substitutions dope low density charge carriers of $2p$ character. These charge carriers are partially localized (binding energy $\sim$15 meV) due to disorder and are responsible for ferromagnetism. It is noted here that ferromagnetism due to $2p$ electrons has been predicted in other systems such as C impurities in BN nanotubes [27].

In summary, high resolution spectra of ferromagnetic CaB_6 exhibit a finite density of states at ϵ_F and emergence of distinct weakly localized features below ϵ_F, which is not observed in paramagnetic LaB_6. The details of the temperature evolutions of the high resolution spectra suggest that there are two parameters that are important to derive ferromagnetism in hexaborides: disorder in the B sublattice and conduction electron density.

The authors acknowledge discussions with Professor S. Das Sarma and Professor A. Fujimori. One of the authors, S. P., thanks the Council of Scientific and Industrial Research, Government of India for financial support.

*kbmaiti@tifr.res.in

[1] P. Vonlanthen *et al.*, Phys. Rev. B **62**, 10076 (2000).
[2] H. R. Ott *et al.*, Physica (Amsterdam) **281B&282B**, 423 (2000).
[3] D. P. Young *et al.*, Nature (London) **397**, 412 (1999).
[4] S. Massidda, A. Continenza, T. M. de Pascale, and R. Monnier, Z. Phys. B **102**, 83 (1997).
[5] D. Ceperley, Nature (London) **397**, 386 (1999).
[6] M. E. Zhitomirsky, T. M. Rice, and V. I. Anisimov, Nature (London) **402**, 251 (1999); M. E. Zhitomirsky and T. M. Rice, Phys. Rev. B **62**, 1492 (2000).
[7] R. G. Goodrich *et al.*, Phys. Rev. B **58**, 14896 (1998).
[8] M. C. Aronson *et al.*, Phys. Rev. B **59**, 4720 (1999).
[9] D. Hall *et al.*, Phys. Rev. B **64**, 233105 (2001).
[10] H. J. Tromp *et al.*, Phys. Rev. Lett. **87**, 016401 (2001).
[11] J. D. Denlinger *et al.*, Phys. Rev. Lett. **89**, 157601 (2002).
[12] S. Souma *et al.*, Phys. Rev. Lett. **90**, 027202 (2003).
[13] K. Matsubayashi *et al.*, Nature (London) **420**, 143 (2002).
[14] T. Morikawa, T. Nishioka, and N. K. Sato, J. Phys. Soc. Jpn. **70**, 341 (2001).
[15] J.-S. Rhyee and B. K. Cho, J. Appl. Phys. **95**, 6675 (2004).
[16] R. Monnier and B. Delley, Phys. Rev. Lett. **87**, 157204 (2001).
[17] D. M. Edwards and M. Katsnelson, J. Phys. Condens. Matter **18**, 7209 (2006).
[18] S. E. Lofland *et al.*, Phys. Rev. B **67**, 020410(R) (2003).
[19] We verified that the spectra obtained from scraped and fractured surfaces are identical.
[20] P. Blaha, K. Schwarz, G. K. H. Madsen, D. Kvasnicka, and J. Luitz (WIEN2k), *An Augmented Plane Wave + Local Orbitals Program for Calculating Crystal Properties* (Karlheinz Schwarz, Technische Universität Wien, Austria, 2001), ISBN .
[21] L. Hedin, Phys. Rev. **139**, A796 (1965); L. Hedin, J. Phys. Condens. Matter **11**, R489 (1999).
[22] K. Maiti *et al.*, Phys. Rev. Lett. **95**, 016404 (2005).
[23] K. Maiti *et al.*, Phys. Rev. B **70**, 195112 (2004).
[24] B. L. Altshuler and A. G. Aronov, Solid State Commun. **30**, 115 (1979).
[25] V. R. R. Medicherla, S. Patil, R. S. Singh, and K. Maiti, Appl. Phys. Lett. **90**, 062507 (2007).
[26] G. Schell, H. Winter, H. Rietschel, and F. Gompf, Phys. Rev. B **25**, 1589 (1982); H. G. Smith *et al.*, Solid State Commun. **53**, 15 (1985); K. Takegahara and T. Kasuya, Solid State Commun. **53**, 21 (1985).
[27] R. Wu, G. Peng, L. Liu, and Y. P. Feng, arXiv:condmat/0501104.